Application of fluorescence polarization microscopy to measure fluorophore orientation in the outer hair cell plasma membrane

Jennifer N. Greeson
Robert M. Raphael
Rice University
Department of Bioengineering
MS 142, P.O. Box 1892
Houston, Texas 77251-1892
E-mail: rraphael@rice.edu

Abstract. The biophysical properties and organization of cell membranes regulate many membrane-based processes, including electromotility in outer hair cells (OHCs) of the cochlea. Studies of the membrane environment can be carried out by measuring the orientation of membrane-bound fluorophores using fluorescence polarization microscopy (FPM). Due to the cylindrical shape of OHCs, existing FPM theory developed for spherical cells is not applicable. We develop a new method for analyzing FPM data suitable for the quasi-cylindrical OHC. We present the theory for this model, as well as a study of the orientation of the fluorescent probe pyridinium, 4-[2-[6-(dioctylamino)-2-naphthalenyl]ethenyl]-1-(3-sulfopropyl) (di-8-ANEPPS) in the OHC membrane. Our results indicate that the absorption transition dipole moment of di-8-ANEPPS orients symmetrically about the membrane normal at 27 deg with respect to the plane of the membrane. The observed agreement between theoretical predictions and experimental measurements establishes the applicability of FPM to study OHC plasma membrane properties. [DOI: 10.1117/1.2717499]

Keywords: molecular orientation; di-8-ANEPPS; membrane order; lipid-protein interactions; prestin.

Paper 06207SSRR received Aug. 3, 2006; revised manuscript received Dec. 20, 2006; accepted for publication Jan. 16, 2007; published online Apr. 3, 2007.

1 Introduction

The importance of the cell membrane environment in regulating biological function has become increasingly evident. Originally thought to serve simply as a barrier between the cell and its external environment, the plasma membrane is now implicated in relaying most of the external signals a cell sends or receives.[1] One useful method for probing the membrane environment is the study of membrane-bound fluorophore orientation. The orientation of membrane molecules is important in defining the structure and electrostatic behavior of the membrane. For example, phospholipid headgroup orientation has shown sensitivity to the presence of both ions and amphiphilic molecules as demonstrated by nuclear magnetic resonance spectroscopy (NMR)[2,3] and molecular dynamics simulations.[4,5] Moreover, changes in the orientation of membrane molecules have been linked to many biological processes such as cell membrane fusion,[6,7] and recent reports suggest that the membrane environment plays a direct role in mediating protein function.[8–10]

In the cochlea, outer hair cells (OHCs) display a protein-driven, membrane-mediated electromechanical transduction process.[11,12] The OHC is a unique, sensory epithelial cell that responds to transmembrane potential changes through axially directed whole cell deformations.[13–15] This process, termed electromotility, is thought to play a role in the active mechanism necessary to obtain the sensitivity and frequency selectivity of mammalian hearing.[11,12,16,17] The electromotile response is initiated in the OHC plasma membrane[18,19] either directly or indirectly through the transmembrane protein prestin.[17,20] However, details of the molecular mechanism of electromotility and the role of the plasma membrane remain elusive.

Electromotility is sensitive to the presence of both hydrophobic ions (Cl^-, I^-, and Br^-) or the amphiphilic metabolite of aspirin, salicylate.[21,22] In the case of salicylate, there is speculation that this small, polar molecule acts as a competitive antagonist to intracellular Cl^- ions.[23] Yet evidence in synthetic membranes suggests that salicylate acts directly on the membrane and disrupts stability by reducing membrane bending stiffness and thickness.[24] Additionally, reports have demonstrated prestin oligomerization,[25–27] and recent evidence indicates these prestin-prestin interactions depend on membrane cholesterol composition (data not presented here). In addition to membrane composition, membrane curvature can also play an important role in mediating protein-protein interactions.[28] Thus, the ability to correlate OHC membrane behavior with the orientation of constituent molecules will further elucidate the role of the plasma membrane environment in mediating both prestin function and OHC electromotility.

Address all correspondence to Robert Raphael, Department of Bioengineering, Rice University, Dept of BioE, MS-142 - PO Box 1892, Houston, Texas 77251 United States of America; Tel: 713-348-3494; Fax: 713-348-5877; E-mail: rraphael@rice.edu

1083-3668/2007/12(2)/021002/9/$25.00 © 2007 SPIE

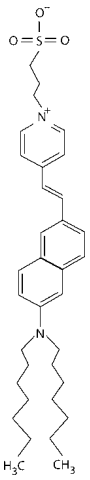

Fig. 1 Structure of di-8-ANEPPS.

Fluorescence polarization microscopy (FPM) is a powerful technique that exploits the anisotropy of fluorescent molecules to discern information about the orientation of membrane-embedded probes. The original theory for FPM was developed by Axelrod to study the orientation of 3,3′-dioctadeylindocarbocyanine diI-C_{18}-(3) (diI) in sphered red blood cells.[29] We previously applied FPM to study membrane fluorophore orientation in synthetic, giant unilamellar vesicles (GUVs),[30] and other laboratories used similar theories to study actin orientation in red blood cells[31,32] and muscle.[33,34] Because the technique can be carried out in live cells, dynamic studies are also possible. FPM thus has the potential to correlate the orientational order of the membrane with physiological processes.

In this study, we utilize FPM to investigate the orientation of a lipophilic dye molecule, pyridinium, 4-[2-[6-(dioctylamino)-2- naphthalenyl]ethenyl]-1-(3-sulfopropyl) (di-8-ANEPPS), in the OHC plasma membrane. Di-8-ANEPPS (Fig. 1) was originally developed in the Loew laboratory as a voltage-sensitive membrane probe.[35] The absorption transition dipole moment of di-8-ANEPPS is predicted to be in the plane of the conjugated ring system, directed along the axis connecting the pyridinium and napthyl nitrogens.[36,37] When di-8-ANEPPS absorbs energy and is elevated to an excited state, the positive charge centered about the pyridinium nitrogen transfers to the naphthyl nitrogen. Interactions between the transmembrane electric field and the transition dipole moments of the fluorophore induce a spectral shift of the emission.[37–39] Thus, the membrane dipole potential can be measured through quantization of these potential-sensitive fluorescence spectra shifts.[40–42]

In cell membranes, di-8-ANEPPS interdigitates with lipid molecules, aligning with their polar and nonpolar regions and shows minimal internalization.[39] In OHCs, di-8-ANEPPS labels the plasma membrane effectively and selectively[43] and has been used in several studies of lateral diffusion in OHCs.[44–46] The diffusion of di-8-ANEPPS in the OHC membrane has shown sensitivity to voltage and ionic amphipaths, and these effects have been attributed to nanoscale rippling of the OHC membrane.[45,47] In addition, recent results indicate that di-8-ANEPPS lateral diffusion is anisotropic and that this anisotropy may be mediated by interactions with the underlying cytoskeleton of the OHC trilaminate lateral wall structure.[46] Quantifying the orientation of di-8-ANEPPS in the OHC lateral wall can lead to a deeper understanding of these experimental observations.

We begin here with a presentation of FPM theory developed specifically for use in analyzing the orientation of a membrane probe in the cylindrical OHC. This required an extension of the original FPM theory developed for a spherical sample.[29] We then describe FPM experiments conducted in living OHCs. Comparing theoretical orientation predictions with experimental results, we can predict two parameters: the orientation of the absorption transition dipole moment of di-8-ANEPPS with respect to the plane of the OHC membrane (θ) and the fraction of oriented molecules (OF). Knowledge of both θ and OF provides insight into a number of physical properties of the membrane, such as stability and organization.

2 Fluorescence Polarization Microscopy

FPM utilizes polarized light to determine the orientation of the absorption and emission transition dipole moments of a fluorescent molecule. The technique exploits the anisotropy of fluorescent molecules, which is defined as the degree of emission polarization from a sample excited with polarized light.[48] A fluorescent molecule will be preferentially excited if its absorption transition dipole moment is aligned with the polarization of the incoming light. If the transition dipole moment is misaligned, the absorption is equivalent to the squared cosine of the angle between the transition dipole moment and the polarization vector. If the fluorescent intensity from this fluorophore is measured after passing the emission through a second polarizer, or analyzer, oriented either parallel or orthogonal to the excitation polarization, the orientation of the dipole can be calculated. This calculation is straightforward, since the intensity measured is simply the projection of the electric field of the molecule's transition dipole moment onto the transmission axis of the analyzer.[48] Thus, an orientation-dependent, theoretical prediction for fluorescent intensity can be validated through experimental measurements. This theory for a single transition dipole moment can be extended to a collection of transition dipole moments oriented on a sample, such as fluorophores in a cell membrane.

2.1 *Cylindrical Geometry Theory*

To apply FPM to the OHC, we have developed a cylindrical-sample specific FPM model. Several factors are important in defining a model for fluorophore orientation in a sample: the effect of high numerical aperture optics, the difference between fluorophore absorption and emission transition dipole moments, consideration of the range of fluorophore orientations in a measurement region, and the optical resolution limit. Each of these factors has been discussed at length previously,[29] so only those directly affected by the use of a cylindrical sample are explained in detail here. The generalized equation for the total fluorescence from a sample is shown in Eq. (1), where $m(\Omega,\mu)$ is a weighting function describing the distribution or density of excited fluorophores. This equation can be rewritten more specifically based on analyzer orientation, Eq. (2).

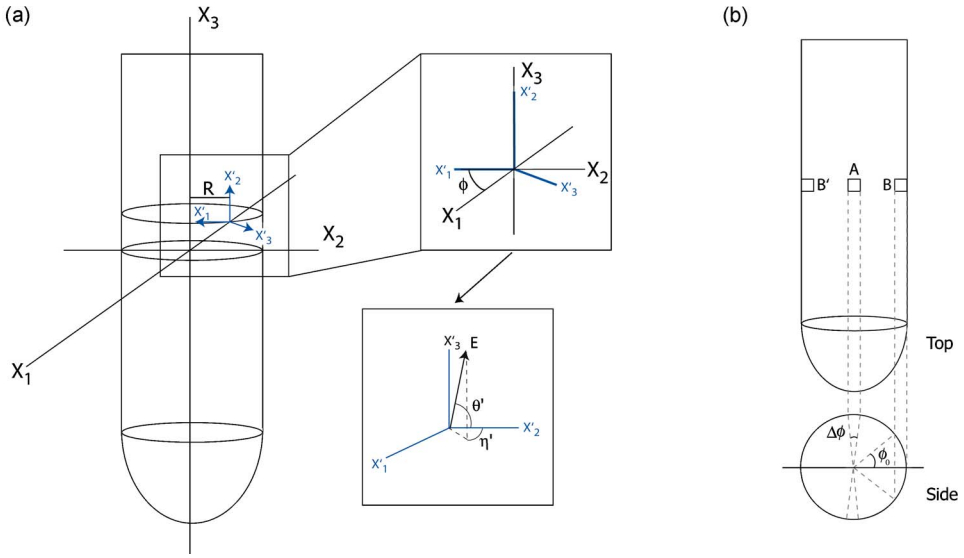

Fig. 2 (**a**) Graphical depiction of two coordinate systems defined for the cylindrical FPM model. The x coordinate system is the sample frame of reference. The x' system is the dipole or fluorophore frame of reference. The angle ϕ indicated in the top inset is a rotation angle used to translate the fluorophore frame of reference into the sample frame of reference. The bottom inset shows the predicted orientation of the emission transition dipole moment of di-8-ANEPPS in the fluorophore frame of reference. (**b**) OHC FPM intensity measurement regions. Shown here are top-down and side views of an imaged OHC. $\Delta\phi$ and ϕ_0 are angles of integration represented generically by s in the FPM model.

$$F_{\perp,\parallel}(\mu) = \int_s \int_\Omega m(\Omega,\mu) I_{\perp,\parallel} \mathrm{d}\Omega \mathrm{d}s, \tag{1}$$

$$F_\perp(\mu) = K_a J_1(\mu) + K_c J_2(\mu) + K_b J_3(\mu)$$

$$F_\parallel(\mu) = K_a J_1(\mu) + K_b J_2(\mu) + K_c J_3(\mu). \tag{2}$$

Here, the subscript on F denotes the orientation of the emission polarizer. In these generalized equations, the parameter μ represents all the constant parameters of the fluorophore, such as the angle between absorption and emission transition dipole moments and rotational diffusion rate. In contrast, the parameter Ω represents all angular variables such as the angles associated with anisotropic excitation and orientation angles over which integration occurs. s is a general parameter that relates to sample size. $I_{\perp,\parallel}$ are the fluorescent intensities of a single transition dipole moment as measured through the two orientations of the emission polarizer. The optical system dependent K parameters are included to account for the effect of high numerical aperture on polarized light and have been defined previously.[29,49] The J parameters, which relate to the distribution of excited fluorophores, are sample dependent and are the source for the most drastic changes between the spherical and cylindrical FPM models. The generalized equation for the J parameters is shown in Eq. (3), where x_i corresponds to one of three coordinates for emission transition dipole moment orientation.

$$J_i(\mu) = \int_s \int_\Omega m(\Omega,\mu) x_i^2 \mathrm{d}\Omega \mathrm{d}s. \tag{3}$$

To develop a specific model of fluorophore orientation on a cylindrical sample, we must define two frames of reference, a fluorophore frame of reference (X') and a sample frame of reference (X), as shown in Fig. 2(a) The fluorophore frame of reference is defined such that X_3' resides along the membrane normal. In the fluorophore frame of reference, the coordinates of the emission transition dipole moment are [see Fig. 2(a) (inset) for angle definitions]:

$$x_1' = \sin\,\eta' \cos\,\theta'$$

$$x_2' = \cos\,\eta' \cos\,\theta'$$

$$x_3' = \sin\,\theta'. \tag{4}$$

Expression of these coordinates in the sample frame of reference requires two transformations: 90 deg about X_1' and, subsequently, $-\phi$ about X_3' [Fig. 2(a)]. The resulting components of the emission transition dipole moment are:

$$x_1 = \sin\,\eta' \cos\,\phi \cos\,\theta' - \sin\,\theta' \sin\,\phi$$

$$x_2 = \sin\,\theta' \cos\,\phi + \sin\,\eta' \cos\,\theta' \sin\,\phi$$

$$x_3 = -\cos\,\eta' \cos\,\theta'. \tag{5}$$

By substituting θ for θ' and η for η', this set in Eq. (5) can also represent the coordinates for the absorption transition dipole moment. The excited molecule orientation distribution for a molecule oriented at η_0 on excitation and at η on emission at Δt time later is:

Table 1 FPM parameters used in the definition of excited molecule orientation density [Eq. (6)]. We estimated the fluorescence lifetime (τ) of di-8-ANEPPS as the lifetime of a similar dye molecule in a membrane.[52,59,60] Additionally, the rotational diffusion coefficient of di-8-ANEPPS was assumed to be equivalent to the rotational diffusion of a lipid in a model membrane.[61]

Parameter	Description
τ	Fluorophore lifetime
β_0	Angle between absorption dipole and excitation polarization direction
$\cos^2\beta_0$	Equivalent to x_3^2 with $\theta'=\theta$ and $\eta'=\eta_0$
$p(\Delta\eta,\Delta t)$	Solution to the rotational diffusion equation: $p(\Delta\eta,\Delta t)=1/2\pi+1/\pi\sum_{k=1}^{\infty}\exp(-k^2D\Delta t)\cos(k\Delta\eta)$, where D is the rotational diffusion constant.

$$m(\Omega,\mu)=\frac{1}{\tau}\int_{\eta_0=-\pi}^{\pi}\int_{\Delta t=0}^{\infty}\cos^2\beta_0 p(\Delta\eta,\Delta t)\exp^{(-\Delta t/\tau)}\mathrm{d}\eta_0\mathrm{d}\Delta t. \tag{6}$$

The remaining parameters in this equation are defined in Table 1. We evaluate this function at the two points on the cylindrical OHC where we wish to take intensity measurements and make predictions, region A ($\phi=\pi/2$) and region B ($\phi=0$) [see Fig. 2(b)]. Since there is no ϕ dependence in the $\cos^2\beta_0$ term, the weighting function is the same at both locations.

$$m(\Omega,\mu)=\frac{\cos^2\theta}{2}\left[1+\frac{\cos(2\eta)}{1+4D\tau}\right]. \tag{7}$$

We can now evaluate our sample-dependent J parameters by combining Eqs. (3), (5), and (7). For region A, we integrate over $\Delta\phi$ around $\phi=\pm\pi/2$, resulting in:

$$J_1=\frac{\Delta\phi}{2}\cos^2\theta\sin^2\theta'$$

$$J_2=\frac{\Delta\phi}{4}\cos^2\theta\cos^2\theta'\left[1-\frac{\cos(2\psi)}{2(1+4D\tau)}\right]$$

$$J_3=\frac{\Delta\phi}{4}\cos^2\theta\cos^2\theta'\left[1+\frac{\cos(2\psi)}{2(1+4D\tau)}\right]. \tag{8}$$

For region B, we integrate between $-\phi_0<\phi<\phi_0$, resulting in:

$$J_1=\frac{\phi_0}{2}\cos^2\theta\cos^2\theta'\left[1-\frac{\cos(2\psi)}{2(1+4D\tau)}\right]$$

$$J_2=\phi_0\cos^2\theta\sin^2\theta'$$

$$J_3=\frac{\phi_0}{2}\cos^2\theta\cos^2\theta'\left[1+\frac{\cos(2\psi)}{2(1+4D\tau)}\right]. \tag{9}$$

Here ψ represents the orientation of the axis connecting the pyridinium and napthyl rings with respect to the plane of the acyl chains. It is also equivalent to the difference between the azimuthal angles that define the orientation of di-8-ANEPPS's emission and absorption transition dipole moments, η' and η, respectively, indicating that rotation of the molecule during the excited state occurs in the plane of the membrane's acyl chains. Combining Eq. (8) or (9) with Eq. (2) yields predictions of the fluorescent intensity in each polarization direction as a function of the molecular orientation of the fluorophore with respect to the membrane. A series of intensity ratios is then calculated using intensity predictions from regions A and B (10). The use of ratios eliminates concentration dependence and allows for cell-to-cell comparison. Here, the superscript denotes the region on the cell and the subscript denotes the orientation of the emission polarizer.

$$\frac{F_\perp^A}{F_\parallel^A},\frac{F_\perp^B}{F_\parallel^B},\frac{F_\parallel^A}{F_\parallel^B},\frac{F_\perp^A}{F_\perp^B},\frac{F_\perp^A}{F_\parallel^B},\frac{F_\perp^B}{F_\parallel^A}. \tag{10}$$

Experimental measurements of these ratios are used to validate the theoretical model for dye orientation. Mathematically, this reduces to a multiparameter minimization problem.

2.2 *Optimization of the Fluorescence Polarization Microscopy Model*

Optimization of the FPM model is carried out using the genetic algorithm tool in Matlab. Genetic algorithms are used to optimize solutions to search problems using techniques inspired by evolutionary biology. In searching for an optimal solution, an initial population is stochastically generated. Members of this population are chosen to reproduce and generate a new population that maintains some characteristics of the initial population. This selection and reproduction continues until an optimized solution is met, as determined by minimizing the fitting function value. In our optimization, the fitting function utilized was the sum of squared errors in prediction for each of the five ratios weighted by the corresponding standard deviation of measurement. Defining the error as such insures that ratios with larger measurement error do not inappropriately skew final angle determination.

Two parameters remain variable in our optimization, the di-8-ANEPPS orientation angle (θ) and the oriented fraction (OF). As defined thus far, the FPM theory assumes all di-8-ANEPPS molecules maintain the same orientation. In a biological system, adherence to this assumption is unlikely, as some molecules will interact with plasma membrane constituents resulting in orientations different from the ensemble. To account for these variable orientations, a portion of di-8-ANEPPS molecules is permitted random orientations, and the remainder of the population, the OF, maintains the orientation predicted by the model. Previously, the randomized population, 1-OF, was set to match immobile fractions measured using fluorescence recovery after photobleaching (FRAP).[29] While defining the parameter in this manner is intuitive, allowing the OF to vary freely broadens its scope. In this work, no initial constraints were placed on the range of OF. This

change in definition allows *OF* to also act as a reporter of membrane order and stability, since highly ordered, stable membranes might restrict fluorophore orientation more than their destabilized counterparts.

3 Materials and Methods

3.1 *Outer Hair Cell Isolation and Loading*

OHCs are obtained from guinea pigs (Charles River, Willmington, Massachusetts). Females ranging in weight from 170 to 230 g are decapitated, and both temporal bones are excised. Portions of the temporal bone and otic capsule are removed to expose the top two turns of the cochlea. Dissection is done with the bone and cochlea bathed in extracellular (EC) solution (140-mM NaCl, 5-mM KCl, 10-mM HEPES 4-(2-hydroxyethyl)-1-piperazineethanesulfonic acid, 10-mM glucose, 1-mM $MgCl_2$, 2-mM $CaCl_2$, ~290 to 300 mOsm, pH 7.3). Once two turns are exposed, the cochlea is placed in EC solution loaded with 150-μM di-8-ANEPPS (Invitrogen Molecular Probes, Carlsbad, California) and incubated at room temperature for 20 min. After incubation, the cochlea is bathed in fresh EC solution, and OHCs are removed from the cochlear tissue through mechanical dissociation.

3.2 *Acquisition of Flourescence Polarization Microscopy Images*

FPM images are obtained on a Zeiss Axiovert 200M microscope using a cooled charge-coupled device (CCD) camera (Axiocam), both operated by Zeiss Axiovision 3.0 software. Appropriate polarizers are inserted into prefabricated slots on the microscope. A slider containing a vertical, linear polarizer shielded by two neutral density filters is placed directly between the mercury arc lamp source and the fluorescence filter wheel. A second slider containing two linear polarizers, one vertical and one horizontal, is placed just before the camera. The polarizers are oriented to achieve maximal light transmission when parallel, and maximal attenuation when orthogonal.

OHCs are chosen for FPM imaging based on standard health characteristics and additional factors necessary for this particular technique. First, the cell must have a basally located nucleus, show no signs of internal Brownian motion, and have negligible cytosolic fluorescence. In addition, the OHC must maintain a rigid, cylindrical shape, and its long edges must be brought into alignment with the vertical axis of the optical system. Once a cell meets these criteria, two images are obtained. The first is taken with the emission polarizer parallel to the excitation polarizer. In the second image, the emission polarizer is oriented orthogonal to the excitation polarizer. The exposure time for each image is constant and is defined using the software's built-in measurement function when the parallel image is obtained. Exposure times ranged from 2 to 8 s for each image pair.

After acquisition, appropriate length scaling is applied to the image, and the diameter of the OHC is measured. Digital apertures (0.97 μm^2, 36 $pixels^2$) are placed on the cell at points A, B, and B′ [see Figs. 2(b) and 3(g)] for intensity measurements. Measured values at B and B′ are averaged to exploit OHC symmetry and decrease measurement noise. FPM ratios (10) are calculated using experimentally measured

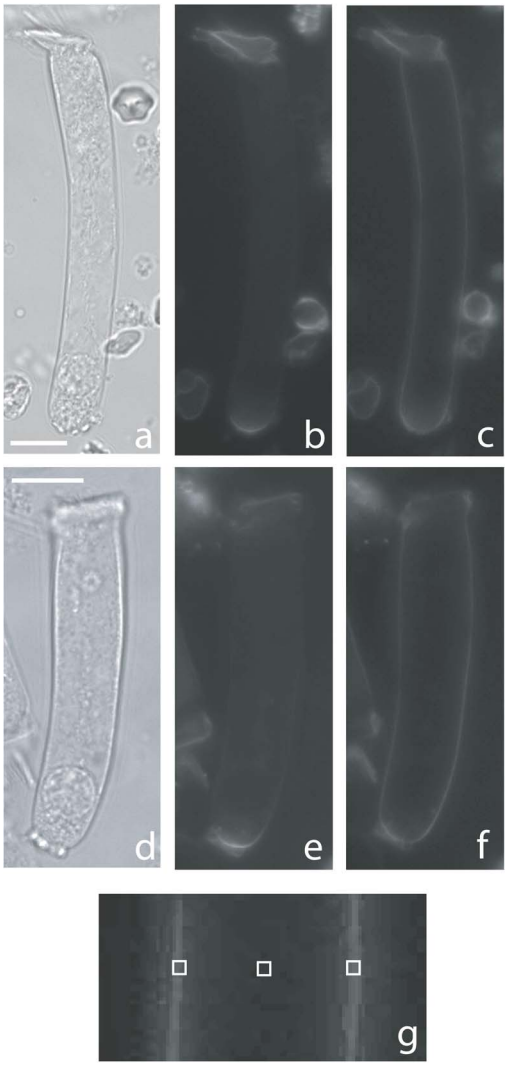

Fig. 3 OHC FPM images. (**a**) and (**d**) Transmitted light images. The scale bar corresponds to 10 μm. (**b**) and (**e**) Images taken with an emission polarizer parallel to the excitation polarizer. (**c**) and (**f**) Images taken with an emission polarizer orthogonal to the excitation polarizer. In all polarization images, the excitation polarization is linear and in the plane of the image along the long axis of the OHC. Exposure times ranged from 2 to 8 s. (**g**) Close-up of FPM intensity measurement regions corresponding to Fig. 2(b).

intensity values for each cell, and averages among the entire cell pool are used for comparison with theoretical predictions of the FPM ratios.

3.3 *Microscope Calibration*

Since microscope optics do not pass orthogonal polarizations with the same efficiency, we have performed appropriate calibrations to insure that measured intensities from FPM images are accurate. The anisotropy (r) of di-8-ANEPPS in chloroform (10 mg/L) was measured on the microscope used, and compared to an anisotropy value obtained using the anisotropy measurement function of a Jobin Yvon fluorometer (r=0.006). Discrepancy between these values was used to generate a calibration factor, or G factor, applied to all measurements from the image obtained with perpendicular

polarizers.[48] A G factor specific to each day of experimentation was generated and ranged from 1.5 to 2.2.

3.4 *Measurement of Angle between Absorption and Emission Transition Dipole Moments*

The angle between the absorption and emission transition dipole moments of a fluorophore (β') can be measured experimentally using randomly oriented, immobilized fluorophores. To achieve this condition, 0.5 mL of di-8-ANEPPS dissolved in chloroform (1 mg/ml) was spread onto a glass coverslip. The chloroform was allowed to evaporate, and a thin layer of agarose gel was placed on top to immobilize the remaining di-8-ANEPPS molecules. FPM images were taken of this plane of fluorescence, and following theory described previously,[29] the angle β' was calculated.

4 Results

FPM was used to analyze the orientation of di-8-ANEPPS in OHCs. Additionally, studies of randomly oriented, immobilized di-8-ANEPPS molecules were conducted to determine the angle between the absorption and emission transition dipole moments β' of the fluorophore. Data from five immobilization samples yielded a difference angle of ±1.08 radians or ±61.9 deg.

For OHC FPM, a total of 17 cells were analyzed. Sample OHC FPM images are shown in Fig. 3 and are indicative of all cells investigated in this study. A qualitative look at these images yields a considerable amount of information. First, because the apical and basal portions of the cell are highlighted in the parallel images [Figs. 3(b) and 3(e)], we can conclude that the di-8-ANEPPS emission transition dipole moment lies approximately perpendicular to the plane of the membrane. Second, the contrast between the parallel and perpendicular images indicates that di-8-ANEPPS maintains a preferred orientation. If the molecules were completely randomly oriented, no differences would be expected between the two FPM images.

Following implementation of our FPM optimization algorithm, it became apparent that the ratio $F_{\perp}^{A}/F_{\parallel}^{A}$ was less sensitive to θ and OF than the remaining five ratios. This decreased sensitivity is evident in Fig. 4, which shows individual ratio values as a function of θ, assuming a constant OF. As such, we have chosen to eliminate the ratio $F_{\perp}^{A}/F_{\parallel}^{A}$ from the final FPM data analysis. Utilizing the remaining five ratios, the cylindrical FPM model is capable of predicting di-8-ANEPPS orientation within 18% error for each individual ratio (Table 2).

The determination of fluorophore orientation using the FPM model requires definition of a relationship between the orientations of the absorption and emission transition dipole moments of the molecule as well as β', the difference between these angles. There are two ways to define this relationship based on the polar coordinate system, and both were employed. The first assumes that the absorption transition dipole moment is oriented at an angle larger than the emission transition dipole moment, and results in the relationship $\theta' = \theta - \beta'$, where θ' is emission transition dipole moment orientation and θ is absorption transition dipole moment orientation. The second assumes the absorption transition dipole moment is oriented at an angle smaller than the emission transition dipole moment, and results in the relationship $\theta' = \theta + \beta'$. As expected, the results from the two cases are symmetric about the membrane normal. When $\theta' = \theta - \beta'$, we predict θ to be 26.7 deg. When $\theta' = \theta + \beta'$, we predict θ to be 153.3 deg. Both angle values correspond to an OF value of 48.1%, indicating roughly half of di-8-ANEPPS molecules maintain the predicted orientation.

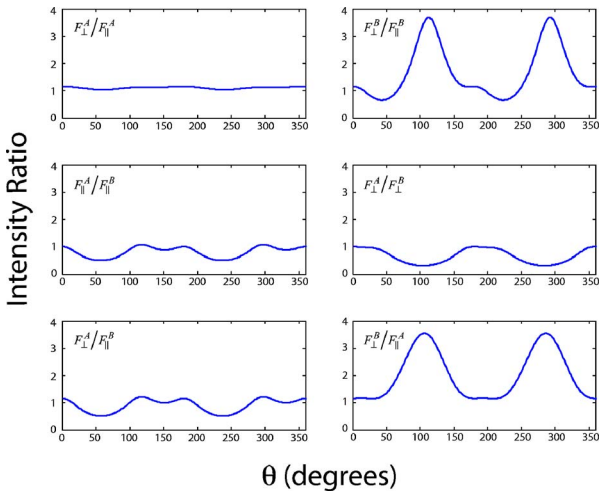

Fig. 4 Individual ratio values as a function of θ. The OF is assumed to be 48.1%, as determined through optimization of the FPM model using average intensity ratio values. The decreased sensitivity of $F_{\perp}^{A}/F_{\parallel}^{A}$ is evidenced by a nearly constant value for the full range of θ values.

Though genetic algorithms are widely regarded as robust algorithms for minimizations, such as the one performed here, an additional assay was carried out to insure that the minima arrived at were global rather that local. Using the OF result from the genetic algorithm optimization, the fitting function was plotted as a function of θ ranging from 0 to 360 deg. Results from the $\theta' = \theta + \beta'$ case are shown in Fig. 5. Period-

Table 2 Comparison between experimentally measured ratio values and those theoretically predicted using the FPM model (n=17). Values for di-8-ANEPPS absorption transition dipole moment orientation (θ) and (OF) as well as the fitting function value (ffval) are also presented.

Ratio	Experiment	Theory	
		$\theta' = \theta - \beta'$	$\theta' = \theta + \beta'$
$F_{\perp}^{B}/F_{\parallel}^{B}$	1.35 ±0.24	1.38	1.38
$F_{\parallel}^{A}/F_{\parallel}^{B}$	1.02 ± 0.07	0.88	0.88
$F_{\perp}^{A}/F_{\perp}^{B}$	0.66 ± 0.12	0.73	0.73
$F_{\perp}^{A}/F_{\parallel}^{B}$	0.87 ± 0.13	1.00	1.00
$F_{\perp}^{B}/F_{\parallel}^{A}$	1.32 ± 0.24	1.56	1.56
	θ	26.71 deg	153.29 deg
	OF	48.10%	48.10%
	ffval	0.68	0.68

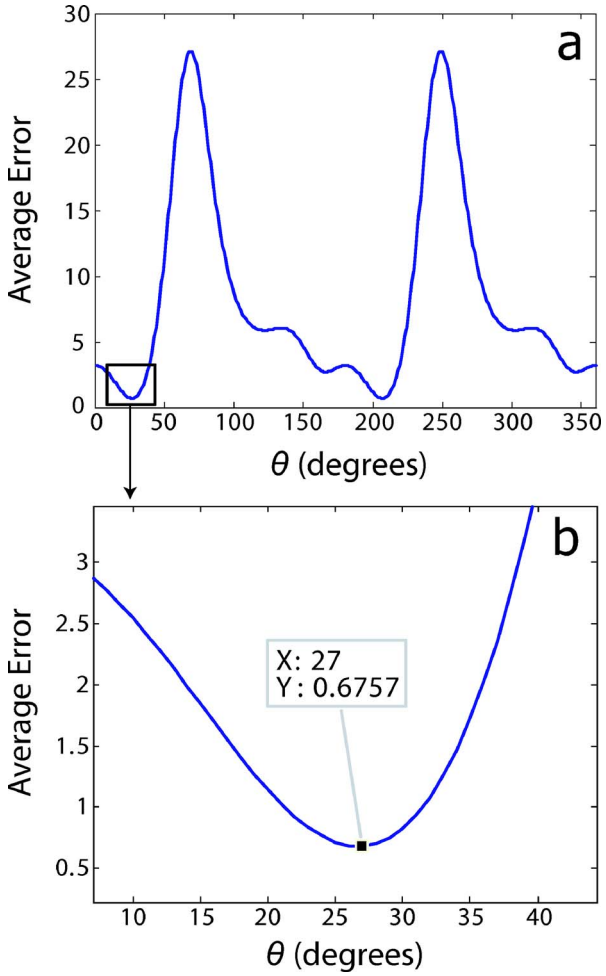

Fig. 5 Average error of FPM model prediction (sum of squared errors weighted by the standard deviation of experimental measurement) as a function of θ. (a) As expected, periodicity about 180 deg is present. One global minima is found at 27 deg as well as two local minima at ~125 and ~170 deg. (b) Close-up of global minima.

icity about 180 deg is present as expected. Also evident is the global minima at 27 deg, which corresponds to results obtained in the genetic algorithm optimization.

5 Discussion

In the study presented here, we have developed an FPM model for membrane fluorophore orientation applicable to cylindrically shaped cells such as auditory and vestibular hair cells. Developing this analysis method required redefining the mathematical equations that describe ensemble fluorophore orientation in a sample, and a genetic algorithm optimization was utilized to match theoretical predictions of intensity ratios to experimentally measured values. The result is a quantitative assessment of di-8-ANEPPS orientation and order in the OHC plasma membrane. In assaying the prediction success of the ratios remaining after exclusion of $F_{\perp}^{A}/F_{\parallel}^{A}$, all five theoretical ratios match to experimental ratios within 18%, and four of the remaining five match within the standard deviation of measurement (Table 2). While even greater agreement between theoretical and experimental values would be ideal, this level of prediction is appropriate for a biological sample. It should also be noted that a similar level of agreement was achieved by Axelrod in his study of diI orientation in the red cell membrane,[29] as well as in our studies of lissamine rhodamine phosphoethanolamine and diI orientation in GUVs.[30]

Based on a qualitative assessment of OHC FPM images (Fig. 3), it appears that the emission transition dipole moment orientation of di-8-ANEPPS is more normal than tangential to the plane of the membrane. From our FPM modeling results, when $\theta' = \theta - \beta'$, θ is 26.7 deg (Table 2). For both of these results to hold, β' must be negative, resulting in a θ' of 88.6 deg. Likewise, when $\theta' = \theta + \beta'$, θ is 153.3 deg, which corresponds to a θ' of 91.4 deg when β' is negative. It is important to note that these two symmetric results are equivalent, as di-8-ANEPPS is constantly undergoing rotational diffusion about its axis normal to the plane of the membrane. This equivalency is validated by the FPM model, which predicts identical ratio values for both cases (Table 2).

Previous reports of di-8-ANEPPS orientation in a pure lipid membrane predict an orientation angle of 36 ± 3 deg[50] and 37.8 ± 1.6 deg[51] with respect to the membrane normal. We predict di-8-ANEPPS orientation to be 26.7 deg from the membrane plane or 63.3 deg from the membrane normal. One potential explanation for this discrepancy is that the previous studies were conducted in synthetic, rather than biological, membranes. Second, in the previous work, the absorption and emission transition dipole moments are presumed to be collinear.[50,51] However, in our findings, the difference angle between the absorption and emission transition dipole moments of di-8-ANEPPS was found to be 61.9 deg. It is likely that this difference angle is the result of a transition from a locally excited state to an intramolecular charge transfer state. During this transition, di-8-ANEPPS molecules undergo rotations to reach equilibrium with the surrounding solvent.[52,53] This process relates to the dependence of the spectral characteristics of di-8-ANEPPS on the polarity of its environment.[52,54]

It is also instructive to note that photoisomerization of di-8-ANEPPS may occur. A recent study demonstrated photoinduced isomerization of another member of the electrochromic family of dye molecules, (E)-4-[2-4-(dihexylamino)phenyl] ethenyl]-1-(4-sulfobutly)-pyridinium (di-6-ASPBS), using high-powered, two-photon laser excitation on the order of 10 to 20 mW.[55] Our system, which utilizes a mercury arc source passed through two neutral density filters and a linear polarizer, cannot achieve these high intensities required to induce a *trans-cis* conformational change in the membrane. Therefore, photoisomerization affects are likely negligible.

In addition to predicting and validating a measure of di-8-ANEPPS orientation in the OHC plasma membrane, the results presented here also offer insight into the extent of di-8-ANEPPS orientation through the prediction of the *OF*. Our FPM model calculates that 48.1% of di-8-ANEPPS molecules in the OHC membrane maintain the predicted ensemble orientation, allowing the other half to maintain randomized orientations. This reduced *OF* may result from the high concentration of protein (roughly 60 to 75% of the membrane[56]) found in the OHC. The incorporation of large amounts of protein into the membrane can have several affects on the

behavior of a probe such as di-8-ANEPPS. For example, a high protein concentration can significantly decrease the fluidity of the membrane,[52] and though a decrease in fluidity might suggest a higher percentage of rigidly oriented di-8-ANEPPS molecules, this idea neglects the behavior of the large fraction of dye molecules that will likely be located at the lipid-protein interfaces, sites of increased curvature in the membrane.[57] Another potential explanation may lie in the nanoscale architecture of the OHC membrane. The membrane-bending model of electromotility postulates that electrically induced membrane curvature changes drive rapid OHC length changes.[47] Nanoscale curvature of the OHC membrane, or rippling, is thought to be present at resting potential, and potentially demonstrates heterogeneity consistent with the heterogeneities seen in the structure of the underlying cytoskeleton.[58] This curvature variation on the membrane scale coupled with curvature at the protein-lipid interface could account for an increase in randomly oriented di-8-ANEPPS molecules.

It is also possible that the lower *OF* measured results from the presence of two or more unique populations of di-8-ANEPPS that maintain different preferred orientations. In tandem FPM studies of fluorophore orientation in GUVs, we have successfully implemented two- and three-state orientation models (data not presented here). Unlike these cases, the application of a two-state orientation model for di-8-ANEPPS in the OHC membrane shows no improvement in error minimization between theory and experiment. As such, we maintain confidence in the existence of a single ensemble orientation for di-8-ANEPPS in the OHC membrane with an equally pervasive randomly oriented fraction.

FPM is an elegant and quantitative optical technique capable of reporting the orientation and *OF* of a fluorophore labeling the membrane. We have presented the first application of FPM to an auditory system cell and laid the groundwork for future applications of this technique to study the OHC membrane response to various perturbations of membrane composition and curvature. The results presented here indicate that the absorption and emission transition dipole moments of di-8-ANEPPS are not collinear as previously assumed.[50,51] We have also demonstrated that despite a relatively large displacement angle during the excited state lifetime, the fluorophore's emission transition dipole moment still maintains the predicted membrane normal orientation. This study has established FPM as a technique for investigating the steady-state orientational order of the OHC plasma membrane that can be utilized to further our understanding of the membrane's role in OHC electromotility.

Acknowledgments

This work is supported by NIH NRSA predoctoral fellowship DC07563-01. Sincerest thanks to Theron Hitchman for his help in understanding the original FPM theory, Imran Quraishi for direction in optimizing the FPM model, Yong Zhou for sharing his knowledge of molecular transition dipole moment behavior, and Louise Organ for technical help and general support.

References

1. J. A. Steyer and W. Almers, "A real-time view of life within 100 nm of the plasma membrane", *Nat. Rev. Mol. Cell Biol.* **2**(4), 268–275 (2001).
2. P. G. Scherer and J. Seelig, "Electric charge effects on phospholipid headgroups. Phosphatidylcholine in mixtures with cationic and anionic amphiphiles," *Biochemistry* **28**(19), 7720–7728 (1989).
3. B. Bechinger and J. Seelig, "Interaction of electric dipoles with phospholipid head groups. A 2H and 31P NMR study of phloretin and phloretin analogues in phosphatidylcholine membranes," *Biochemistry* **30**(16), 3923–3929 (1991).
4. J. N. Sachs and T. B. Woolf, "Understanding the Hofmeister effect in interactions between chaotropic anions and lipid bilayers: molecular dynamics simulations," *J. Am. Chem. Soc.* **125**(29), 8742–8743 (2003).
5. J. N. Sachs, H. Nanda, H. I. Petrache, and T. B. Woolf, "Changes in phosphatidylcholine headgroup tilt and water order induced by monovalent salts: molecular dynamics simulations," *Biophys. J.* **86**(6), 3772–3782 (2004).
6. L. Yang and H. W. Huang, "Observation of a membrane fusion intermediate structure," *Science* **297**(5588), 1877–1879 (2002).
7. L. V. Chernomordik, J. Zimmerberg, and M. M. Kozlov, "Membranes of the world unite!" *J. Cell Biol.* **175**(2), 201–207 (2006).
8. M. Goulian, O. N. Mesquita, D. K. Fygenson, C. Nielsen, O. S. Andersen, and A. Libchaber, "Gramicidin channel kinetics under tension," *Biophys. J.* **74**(1), 328–337 (1998).
9. M. O. Jensen and O. G. Mouritsen, "Lipids do influence protein function—the hydrophobic matching hypothesis revisited," *Biochim. Biophys. Acta* **1666**(1-2), 205–226 (2004).
10. H. T. McMahon and J. L. Gallop, "Membrane curvature and mechanisms of dynamic cell membrane remodelling," *Nature (London)* **438**(7068), 590–596 (2005).
11. D. Z. He, J. Zheng, F. Kalinec, S. Kakehata, and J. Santos-Sacchi, "Tuning in to the amazing outer hair cell: membrane wizardry with a twist and shout," *J. Membr. Biol.* **209**(2-3), 119–134 (2006).
12. A. A. Spector, N. Deo, K. Grosh, J. T. Ratnanather, and R. M. Raphael, "Electromechanical models of the outer hair cell composite membrane," *J. Membr. Biol.* **209**(2-3), 135–152 (2006).
13. W. E. Brownell, C. R. Bader, D. Bertrand, and Y. de Ribaupierre, "Evoked mechanical responses of isolated cochlear outer hair cells," *Science* **227**(4683), 194–196 (1985).
14. B. Kachar, W. E. Brownell, R. Altschuler, and J. Fex, "Electrokinetic shape changes of cochlear outer hair cells," *Nature (London)* **322**(6077), 365–368 (1986).
15. J. F. Ashmore, "A fast motile response in guinea-pig outer hair cells: the cellular basis of the cochlear amplifier," *J. Physiol. (London)* **388**, 323–347 (1987).
16. W. E. Brownell, A. A. Spector, R. M. Raphael, and A. S. Popel, "Micro- and nanomechanics of the cochlear outer hair cell," *Annu. Rev. Biomed. Eng.* **3**, 169–194 (2001).
17. M. C. Liberman, J. Gao, D. Z. He, X. Wu, S. Jia, and J. Zuo, "Prestin is required for electromotility of the outer hair cell and for the cochlear amplifier," *Nature (London)* **419**(6904), 300–304 (2002).
18. F. Kalinec, M. C. Holley, K. H. Iwasa, D. J. Lim, and B. Kachar, "A membrane-based force generation mechanism in auditory sensory cells," *Proc. Natl. Acad. Sci. U.S.A.* **89**(18), 8671–8675 (1992).
19. G. Huang and J. Santos-Sacchi, "Motility voltage sensor of the outer hair cell resides within the lateral plasma membrane," *Proc. Natl. Acad. Sci. U.S.A.* **91**(25), 12268–12272 (1994).
20. J. Zheng, W. Shen, D. Z. He, K. B. Long, L. D. Madison, and P. Dallos, "Prestin is the motor protein of cochlear outer hair cells," *Nature (London)* **405**(6783), 149–155 (2000).
21. S. Kakehata and J. Santos-Sacchi, "Effects of salicylate and lanthanides on outer hair cell motility and associated gating charge," *J. Neurosci.* **16**(16), 4881–4889 (1996).
22. M. Wu and J. Santos-Sacchi, "Effects of lipophilic ions on outer hair cell membrane capacitance and motility," *J. Membr. Biol.* **166**(2), 111–118 (1998).
23. D. Oliver et al. "Intracellular anions as the voltage sensor of prestin, the outer hair cell motor protein," *Science* **292**(5525), 2340–2343 (2001).
24. Y. Zhou and R. M. Raphael, "Effect of salicylate on the elasticity, bending stiffness, and strength of SOPC membranes," *Biophys. J.* **89**(3), 1789–1801 (2005).
25. D. Navaratnam, J. P. Bai, H. Samaranayake, and J. Santos-Sacchi, "N-terminal-mediated homomultimerization of prestin, the outer hair cell motor protein," *Biophys. J.* **89**(5), 3345–3352 (2005).

26. J. N. Greeson, L. E. Organ, F. A. Pereira, and R. M. Raphael, "Assessment of prestin self-association using fluorescence resonance energy transfer," *Brain Res.* **1091**(1), 140–150 (2006).
27. J. Zheng, G. G. Du, C. T. Anderson, J. P. Keller, A. Orem, P. Dallos, and M. Cheatham, "Analysis of the oligomeric structure of the motor protein prestin," *J. Biol. Chem.* **281**(29), 19916–19924 (2006).
28. K. S. Kim, J. Neu, and G. Oster, "Curvature-mediated interactions between membrane proteins," *Biophys. J.* **75**(5), 2274–2291 (1998).
29. D. Axelrod et al., "Carbocyanine dye orientation in red cell membrane studied by microscopic fluorescence polarization," *Biophys. J.* **26**(3), 557–573 (1979).
30. J. N. Greeson and R. M. Raphael, "Orientation of membrane probes in giant unilamellar vesicles," *Proc. SPIE* **5699**, 211–218 (2005).
31. C. Picart and D. E. Discher, "Actin protofilament orientation at the erythrocyte membrane," *Biophys. J.* **77**, 2, 865–878 (1999).
32. C. Picart, P. Dalhaimer, and D. E. Discher, "Actin protofilament orientation in deformation of the erythrocyte membrane skeleton," *Biophys. J.* **79**(6), 2987–3000 (2000).
33. J. Borejdo, D. S. Ushakov, and I. Akopova, "Regulatory and essential light chains of myosin rotate equally during contraction of skeletal muscle," *Biophys. J.* **82**(6), 3150–3159 (2002).
34. J. Borejdo, A. Shepard, D. Dumka, I. Akopova, J. Talent, A. Malka, and T. P. Burghardt, "Changes in orientation of actin during contraction of muscle," *Biophys. J.* **86**(4), 2308–2317 (2004).
35. E. Fluhler, V. G. Burnham, and L. M. Loew, "Spectra, membrane binding, and potentiometric responses of new charge shift probes," *Biochemistry* **24**(21), 5749–5755 (1985).
36. L. Salem, *Molecular Orbital Theory of Conjugated Systems*, Benjamin, Inc., New York (1966).
37. L. M. Loew and L. L. Simpson, "Charge-shift probes of membrane potential: a probable electrochromic mechanism for p-aminostyrylpyridinium probes on a hemispherical lipid bilayer," *Biophys. J.* **34**(3), 353–365 (1981).
38. L. M. Loew, S. Scully, L. Simpson, and A. S. Waggoner, "Evidence for a charge-shift electrochromic mechanismin a probe of membrane potential," *Nature (London)* **281**(5731), 497–499 (1979).
39. L. M. Loew, "Potentiometric dyes: Imaging electrical activity of cell membranes," *Pure Appl. Chem.* **68**(7), 1405–1409 (1996).
40. T. Starke-Peterkovic, N. Turner, M. F. Vitha, M. P. Waller, D. E. Hibbs, and R. J. Clarke, "Cholesterol effect on the dipole potential of lipid membranes," *Biophys. J.* **90**(11), 4060–4070 (2006).
41. R. J. Clarke, "The dipole potential of phospholipid membranes and methods for its detection," *Adv. Colloid Interface Sci.* **89-90**, 263–281 (2001).
42. C. Xu and L. M. Loew, "The effect of asymmetric surface potentials on the intramembrane electric field measured with voltage-sensitive dyes," *Biophys. J.* **84**(4), 2768–2780 (2003).
43. J. S. Oghalai, A. A. Patel, T. Nakagawa, and W. E. Brownell, "Fluorescence-imaged microdeformation of the outer hair cell lateral wall," *J. Neurosci.* **18**(1), 48–58 (1998).
44. J. S. Oghalai, T. D. Tran, R. M. Raphael, T. Nakagawa, and W. E. Brownell, "Transverse and lateral mobility in outer hair cell lateral wall membranes," *Hear. Res.* **135**(1-2), 19–28 (1999).
45. J. S. Oghalai, H. B. Zhoa, J. W. Kutz, and W. E. Brownell, "Voltage- and tension-dependent lipid mobility in the outer hair cell plasma membrane," *Science* **287**(5453), 658–661 (2000).
46. J. B. de Monvel, W. E. Brownell, and M. Ulfendahl, "Lateral diffusion anisotropy and membrane lipid/skeleton interaction in outer hair cells," *Biophys. J.* **91**(1), 364–381 (2006).
47. R. M. Raphael, A. S. Popel, and W. E. Brownell, "A membrane bending model of outer hair cell electromotility," *Biophys. J.* **78**(6), 2844–2862 (2000).
48. J. R. Lakowicz, *Principles of Fluorescence Spectroscopy*, Kluwer Academic/Plenum, New York (1999).
49. P. R. Dragsten, "Mechanism of voltage-induced fluorescence changes of the membrane probe merocyanine 540. A fluorescence polarization study," *Cornell Univ.* (1977).
50. R. S. Ries, H. Choi, R. Blunck, F. Bezanilla, and J. R. Heath, "Black lipid membranes: visualizing the structure, dynamics, and substrate dependence of membranes," *J. Phys. Chem. B* **108**(41), 16040–16049 (2004).
51. A. Lambacher and P. Fromherz, "Orientation of hemicyanine dye in lipid membrane measured by fluorescence interferometry on a silicon chip," *J. Phys. Chem. B* **105**(2), 343–346 (2001).
52. R. J. Clarke and D. J. Kane, "Optical detection of membrane dipole potential: avoidance of fluidity and dye-induced effects," *Biochim. Biophys. Acta* **1323**(2), 223–239 (1997).
53. B. Valeur, *Molecular Fluorescence*, Wiley-VCH, Weinheim, Germany (2002).
54. E. Gross, R. S. Bedlack, and L. M. Loew, "Dual-wavelength ratiometric fluorescence measurement of the membrane dipole potential," *Biophys. J.* **67**(1), 208–216 (1994).
55. T. Pons, L. Moreaux, and J. Mertz, "Photoinduced flip-flop of amphiphilic molecules in lipid bilayer membranes," *Phys. Rev. Lett.* **89**(28 pt 1), 288104 (2002).
56. A. Forge, "Structural features of the lateral walls in mammalian cochlear outer hair cells," *Cell Tissue Res.* **265**(3), 473–483 (1991).
57. R. L. Goforth, A. K. Chi, D. V. Greathouse, L. L. Providence, R. E. Koeppe, II, and O. S. Andersen, "Hydrophobic coupling of lipid bilayer energetics to channel function," *J. Gen. Physiol.* **121**(5), 477–493 (2003).
58. A. A. Spector, M. Ameen, P. G. Charalambides, and A. S. Popel, "Nanostructure, effective properties, and deformation pattern of the cochlear outer hair cell cytoskeleton," *ASME J. Biomech. Eng.* **124**(2), 180–187 (2002).
59. N. V. Visser, A. van Hoek, A. J. Visser, J. Frank, H. J. Apell, and R. J. Clarke, "Time-resolved fluorescence investigations of the interaction of the voltage-sensitive probe RH421 with lipid membranes and proteins," *Biochemistry* **34**(37), 11777–11784 (1995).
60. M. E. Daraio, N. Francois, and D. L. Bernik, "Correlation between gel structural properties and drug release pattern in scleroglucan matrices," *Drug Deliv.* **10**(2), 79–85 (2003).
61. R. W. Pastor, R. M. Venable, and M. Karplus, "Model for the structure of the lipid bilayer," *Proc. Natl. Acad. Sci. U.S.A.* **88**(3), 892–896 (1991).